Determination of spin-wave stiffness in the Fe-Si system using first-principles calculations

Matteo Rinaldi [1,*] Matous Mrovec [1] Manfred Fähnle,[2] and Ralf Drautz [1]

[1]*Interdisciplinary Centre for Advanced Materials Simulation, Ruhr-Universität Bochum, 44801 Bochum, Germany*

[2]*71272 Renningen, Schönblickstraße 95, Germany, former member of the Max Planck Institute for Intelligent System, Stuttgart, Germany*

(Received 21 May 2021; revised 23 July 2021; accepted 26 July 2021; published 6 August 2021)

The behavior of magnetic materials can be simulated at the macroscale using the micromagnetic model whose key parameters, such as exchange stiffness constants and magnetic anisotropies, can be derived from first-principles electronic structure calculations. In this work we employed the Korringa-Kohn-Rostoker (KKR) Green's function method with the coherent potential approximation (CPA) to investigate the dependence of the spin-wave stiffness on the Si concentration for the three magnetic phases of FeSi, namely A2, B2, and $D0_3$. Based on the structural, magnetic, and electronic structure analysis using the KKR-CPA methodology, the changes in the spin-wave stiffness caused by the addition of Si are primarily governed by the variations in the electronic structure.

DOI: 10.1103/PhysRevB.104.064413

I. INTRODUCTION

Magnetic steels containing small amounts of silicon have been used extensively as soft magnetic materials in various technological applications. The addition of Si is crucial for the improvement of intrinsic magnetic properties as well as low core losses, small saturation induction, and high electrical resistivity [1].

The Fe-Si phase diagram [2] in the range of 0–25 at.% of Si is characterized by the presence of three phases: a fully disordered body-centered cubic (bcc) α phase (A2 Strukturbericht crystallographic designation), and two partially ordered α_1 and α_2 phases (corresponding to the $D0_3$ and B2 Strukturbericht designations, respectively) emerging below and above the Curie temperature. The latter two structures correspond to the Fe_3Si and CsCl prototypes with nominal Si concentrations equal to 25 and 50 at.%, respectively. The $D0_3$ structure is composed of four face-centered cubic (fcc) sublattices, usually denominated as A, B, C, and D, displaced along the cube diagonal. Iron atoms occupy the A, B, and C sites while silicon is located at the D sites. The A and C sites are structurally and magnetically equivalent with four Fe and four Si nearest neighbors. The Fe atoms on the B sites have eight first-nearest Fe neighbors like in bulk bcc Fe.

The energetical stability, magnetic properties, and local chemical order of the Fe-rich Fe-Si phases have been investigated extensively in the past by both experiments and theory [3–17]. It has been established that for both ordered and disordered Fe-Si phases, the magnetic moments at different Fe sites are strongly affected by the local atomic environment and the number of Si atoms in the first coordination shells. Already early studies [3–5] revealed the existence of very different magnetic moments on Fe atoms in the $D0_3$ phases. Based on experimental determination of the magnetic moments for alloys with low Si content, Niculescu *et al.* [6] and Elsukov *et al.* [7] formulated a phenomenological model according to which the magnetic moments of Fe atoms decrease linearly with the increasing average number of Si nearest neighbors. Furthermore, more recent experimental studies [12,14] suggested that the induced uniaxial magnetic anisotropy in the Fe-rich Fe-Si alloys (with 5 to 10 at.% of Si) is due to a B2-type short-range order (SRO) formed during the thermomagnetic or thermomechanical treatment, such as annealing and cooling in a constant magnetic field or under external load along the $\langle 100 \rangle$ easy magnetization axis.

The experimental studies have been complemented by numerous electronic structure calculations. Williams *et al.* [8] were the first ones to calculate the Fe magnetic moments in the ordered $D0_3$ phase using rudimentary electronic structure calculations. The first thorough theoretical analysis was carried out by Kudrnovský *et al.* [9] who employed the coherent-potential approximation (CPA) to compute the properties of the $D0_3$ phase using the linear-muffin-tin-orbital (LMTO) framework, where the disorder was introduced on the D sites only. The resulting $Fe_{1-x}Si_x$ magnetic moments for the range of Si concentrations between $0.10 \leqslant x \leqslant 0.25$ showed a decreasing linear behavior for the A and C sites while for the B sites the magnetic moments remained almost constant. Moroni *et al.* [10] investigated the stability and elastic properties of several Fe silicides using a full-potential linearized-augmented-plane-wave (FLAPW) approach. In another study, Kulikov *et al.* [11] employed the Korringa-Kohn-Rostoker (KKR) approach with CPA as well as supercell TB-LMTO calculations to study a fully disordered bcc $Fe_{1-x}Si_x$ and partially ordered $D0_3$ and B2 phases. It was shown that the magnetic energy governs the stability of $D0_3$ over B2 for temperatures below T_C. Moreover, the calculated magnetic moments for the fully disordered structures followed the linear behavior observed by Elsukov *et al.* [7]. However, more recent studies [13,15–17] have revealed that some properties (e.g., bulk modulus, heat of formation) of

*matteo.rinaldi@rub.de

the disordered alloys depend on the details of local electronic structure and cannot be derived by a simple interpolation between a highly diluted Fe-Si solid solution and the ordered $D0_3$ Fe_3Si phase.

A common outcome of all studies mentioned above is the fundamental role played by magnetism in determining the phase stability, SRO, and variations of the bulk modulus in the Fe-rich Fe-Si alloys. The aim of our study is to gain further insight into the interplay between the local atomic structure, chemistry, and magnetism in the dilute Fe-Si alloys by examining additional relevant quantities such as the Heisenberg exchange interactions and the spin-wave stiffness. To the best of our knowledge, no calculations of the spin-wave stiffness have been carried out for the ferromagnetic partially ordered A2, B2, and $D0_3$ Fe-Si phases. Such study is highly desirable as the theoretical understanding of the role played by magnetism, both at the atomic and mesoscopic level, is crucial for the technological important soft magnetic Fe-Si steels.

II. METHODS

A. Theoretical background

When dealing with itinerant magnetic systems at low temperature, it is convenient to map the energy landscape to an Heisenberg-like model Hamiltonian

$$H = -\sum_{i \neq j} J_{ij} \mathbf{S}_i \mathbf{S}_j, \tag{1}$$

which is formulated in terms of local exchange interaction J_{ij} between spins $\mathbf{S}_i$ and $\mathbf{S}_j$ on sites i and j, respectively. This approximate description can be further incorporated in dynamic models of magnetization, both in the atomic-level spin dynamics and mesoscopic-level micromagnetic modeling. The latter involves a coarse-graining of the distribution of magnetic moments under the assumption of local collinearity of atomic magnetic moments to obtain a macroscopic expression for the Gibbs free energy. Among the energy contributions, the exchange term, which is for cubic systems given by

$$E_{\text{exch}} = A \sum_{i=x,y,z} \int_V [\nabla m_i(\mathbf{r})]^2 dV, \tag{2}$$

can be derived from the microscopic Heisenberg Hamiltonian by assuming a continuum distribution of the magnetization in real space. The exchange parameter A, which appears in front of the integral, can be derived from microscopic spin-wave stiffness D through the expression

$$A = \frac{D M_S}{2 g \mu_B}, \tag{3}$$

where M_S is the saturation magnetization, g is the Landé factor, and μ_B is the Bohr magneton. The spin-wave stiffness is an important quantity at the atomic level because it determines the low-temperature magnetic excitations and is related to the curvature of the magnon spectra.

There exist several techniques that can be used to extract the spin-wave stiffness using first-principles calculations (cf. recent reviews by Šipr *et al.* [18] and Turek *et al.* [19]). The method that is used in this work was derived by Liechtenstein and co-workers [20–22]. It essentially relates D with the real space representation of the Heisenberg exchange interactions through the following formula valid for cubic systems:

$$D = \sum_j \frac{2\mu_B}{3\mu_j} J_{0j} R_{0j}^2, \tag{4}$$

where the summation extends up to a converged cutoff radius. The spin-wave stiffness can be also obtained by carrying the summation in reciprocal space, but this involves a numerically expensive evaluation of the derivative of the scattering-path operator with respect to the $\mathbf{k}$ vector [20–22]. Other possible techniques include a spin-spiral approach, where the curvature of the magnon spectra at $\mathbf{q} = \mathbf{0}$ is extracted, or a recently formulated method inspired by the transport theory [19].

B. Computational details

In our study we used the spin-polarized multiple-scattering KKR Green's function approach as implemented in the SPRKKR [23] code. The KKR calculations were performed in the scalar-relativistic mode using the Perdew, Burke, and Ernzerhof (PBE) generalized gradient approximation (GGA) functional within the atomic-sphere approximation (ASA). We employed CPA to simulate the chemical disorder. The chosen angular momentum cutoff was $l_{\max} = 3$. The equilibrium lattice parameters at all concentrations were obtained by fitting the energy-volume curves to the Murnaghan equation of state. The calculations were performed for the fully disordered A2 phase and the partially disordered $D0_3$ and B2 phases with Si concentrations ranging up to 20 at.%. The Heisenberg exchange interactions, which are the key ingredients for the determination of the spin-wave stiffness in Eq. (4), were determined for the three phases employing the Liechtenstein formula [20–22].

To overcome the well-know problems related to the long-range Ruderman-Kittel-Kasuya-Yosida (RKKY) oscillatory behavior of the exchange interactions for transition metals, such as Fe, Co, and Ni, we used the method of Pajda *et al.* [24] generalized to the case of multicomponent systems [25,26]. This method uses an exponential damping to converge the conditionally convergent sum in Eq. (4) as follows:

$$D = \lim_{\eta \to 0} D(\eta), \tag{5}$$

$$D(\eta) = \sum_\alpha c_\alpha D_\alpha(\eta), \tag{6}$$

$$D_\alpha(\eta) = \sum_j \sum_\beta c_\beta \frac{2\mu_B}{3\sqrt{\mu_\beta \mu_\alpha}} J_{0j} R_{0j}^2 \exp(-\eta R_{0j}/a), \tag{7}$$

where α labels the atomic type, c_α is the concentration of type α, μ_α is the corresponding magnetic moment, and η is the damping parameter. Equation (7) is valid only for structures with a single sublattice, such as the A2 phase. For the B2 and $D0_3$ phases, which are composed of two and three sublattices, respectively, the total spin-wave stiffness was computed as a weighted average of the spin-wave stiffness from all distinct lattice sites as

$$D(\eta) = \frac{1}{N} \sum_{\alpha=1}^{N} c_\alpha D_\alpha(\eta), \tag{8}$$

where N is the number of nonequivalent atomic types (two for B2 and four for $D0_3$). The validity of this approximation was tested for the ordered $D0_3$ phase by calculating its spin-wave stiffness from the curvature of the adiabatic magnon spectrum (see the Appendix A). Both methods gave consistent results.

For the B2 phase we also evaluated the total spin-wave stiffness by diagonalizing the full matrix of the sublattice interactions and considering the largest eigenvalue, as was done in Refs. [25,26]. The two approaches gave equivalent results.

For analysis of the spin-wave stiffness variations due to Si addition (see below), we found it useful to consider two partial contributions to the total value of D_α in Eq. (7), namely

$$D_\alpha^{\mathrm{mag}}(x) = \sum_\beta \frac{2\mu_B}{3\sqrt{\mu_\alpha(x)\mu_\beta(x)}} \tag{9}$$

and

$$D_\alpha^{\mathrm{el}}(x,\eta) = c_\alpha(x)\sum_\beta c_\beta(x) \times \sum_j J_{0j}^{\alpha\beta}(x,R_{0j})R_{0j}^2 \exp(-\eta R_{0j}/a). \tag{10}$$

The first contribution $D_\alpha^{\mathrm{mag}}(x)$ has a pure magnetic origin as it only depends on the single-site magnetic moments, which are functions of Si concentration. The second contribution $D_\alpha^{\mathrm{el}}(x)$ is given as a sum of the Heisenberg exchange interactions weighted by the squares of the distances from the origin of the coordination shells. Therefore, it does not depend directly on the magnetic moments but rather on the details of the electronic structure, such as changes of the interactions between the Fe d orbitals induced by the hybridization with the Si p orbitals. The advantage of considering these partial contributions separately is to analyze atomic quantities that can be qualitatively linked to the trends of $c_\alpha D_\alpha$ (see below).

The KKR calculations were performed by extending the summation up to $R_{\max} = 20a$ ($a = 2.8263$ Å is the equilibrium lattice parameter of bcc Fe) and by using a k mesh of $92 \times 92 \times 92$ points in the full Brillouin zone (BZ) for the bcc cell. A fifth order polynomial was used for the extrapolation and η was sampled in the interval [0.2, 1.0]. The convergence of this modified expression for D with respect to the cutoff radius and the k-point mesh has recently been analyzed by Šipr *et al.* [18].

The following naming conventions are used throughout the paper to indicate the different atomic sites in the B2 and $D0_3$ phases: Fe(I) denotes the site occupied partially by Si (corresponding to the D site in $D0_3$ or the central atom in B2), Fe(II) is the Fe atom with Si atoms in the first coordination shell (corresponding to the A and C sites in $D0_3$ or the corner atoms in bcc or B2), and Fe(III) is the Fe atom with Si atoms in the second coordination shell (corresponding to the B sites in $D0_3$). The nonequivalent sites are shown for both phases in Fig. 1.

III. ANALYSIS OF THE RESULTS

A. Analysis of the magnetic moment distribution

The total and site-resolved magnetic moments as functions of Si content computed using the KKR-CPA approach are presented in Figs. 2 and 3, respectively. These trends are comparable with the previous KKR-CPA calculations [11], which analyzed the differences in the total and site resolved magnetic moments for the partially ordered phases and the ordered bcc phase. Our results in Fig. 3 show a strong decrease of the magnetic moments with increasing Si concentration at the Fe(II) sites in both B2 and $D0_3$ phases while the magnetic moments at the Fe(I) and Fe(III) sites slightly increase. A detailed interpretation of these trends is not the focus of this paper and the interested reader is referred to previous studies [9–11].

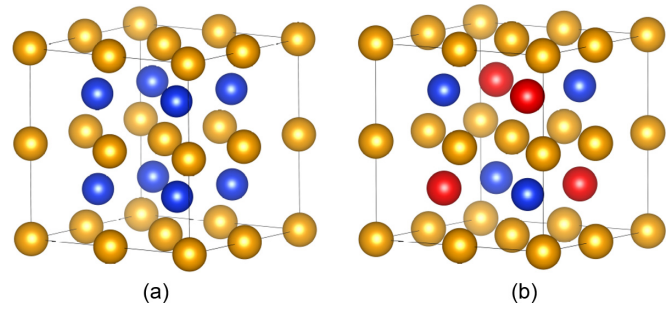

FIG. 1. Atomic structures of the B2 (a) and $D0_3$ (b) phases; the Fe(I), Fe(II), and Fe(III) sites are in blue, orange, and red, respectively.

B. Spin-wave stiffness as a function of the Si concentration

Similarly to magnetic moments, the differences between different sites are emerging also for other fundamental magnetic quantities, such as site-resolved exchange interactions and the spin-wave stiffness for each atomic type. By computing the site-resolved quantities $c_\alpha D_\alpha$ extrapolated to $\eta = 0$ in Eq. (6) one can elucidate contributions of different Fe sites to the total value of D and, hence, to obtain a deeper understanding about the origin of the obtained trends. The variations of the spin-wave stiffness upon doping can be related to changes of the equilibrium volume, changes of the magnetic moments,

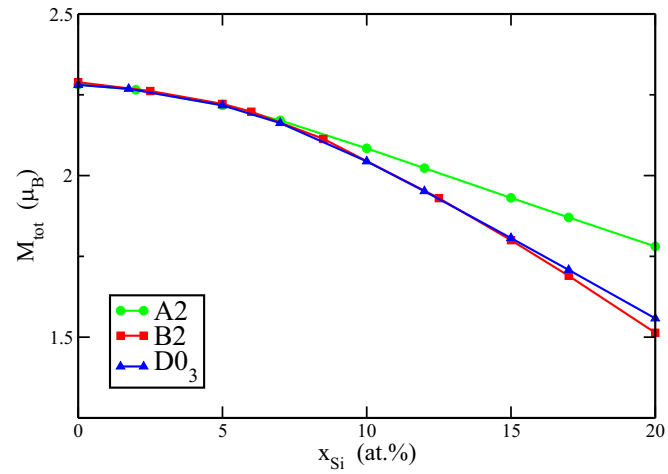

FIG. 2. A comparison of the total magnetization for A2, B2, and $D0_3$ phases as a function of the Si concentration obtained using the KKR-CPA method.

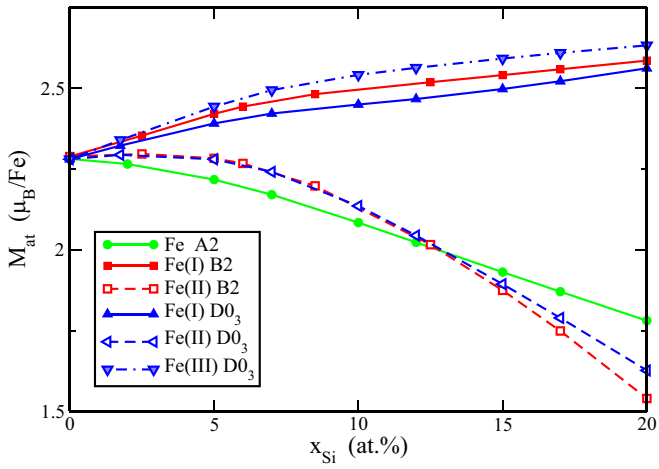

FIG. 3. KKR-CPA magnetic moments for the different sites of the A2, B2, and $D0_3$ phases as a function of the Si concentration.

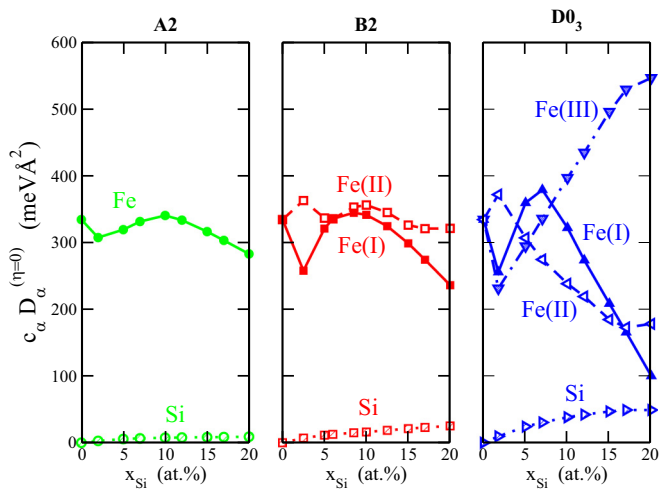

FIG. 5. Site-resolved $c_\alpha D_\alpha$ for different sites of the A2 (left panel), B2 (middle panel), and $D0_3$ (right panel) phases as a function of Si concentration.

or changes of the electronic structure and hybridization mechanisms.

The variations of the total spin-wave stiffness as function of Si content, calculated by interpolating the value of $D(\eta)$ to zero, are shown for all three phases in Fig. 4. The figure also contains results obtained by neglecting all Si contributions in the sum over α and β in Eqs. (6) and (7). One can see that by excluding the Si contributions the qualitative trends are not affected, but the stiffness magnitudes are reduced. This reduction is more pronounced with increasing Si content. Therefore, the induced antiparallel magnetic moment (of about 0.1–0.2 μ_B) on the Si atoms has a small but not negligible effect on the total value of the stiffness as a function of Si concentration.

We included in the graph also available experimental data for the Fe-Si alloys and the range of values for pure Fe obtained by previous theoretical and experimental studies. The

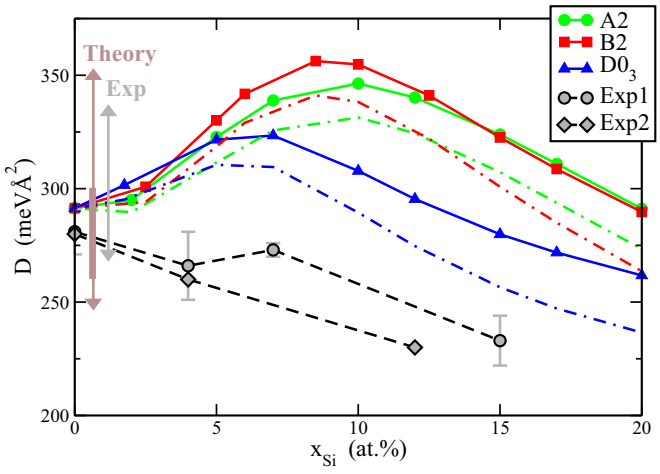

FIG. 4. Spin-wave stiffness for the A2, B2, and $D0_3$ phases as a function of the Si concentration obtained with the KKR-CPA method. The dashed lines were obtained by neglecting all Si contributions in Eqs. (6) and (7). The experimental results are taken from Refs. [27] (Exp1) and [28,29] (Exp2).

site-resolved extrapolated quantities $c_\alpha D_\alpha$ are plotted separately for each phase in Fig. 5. The A2 and B2 phases show very similar trends for the total spin-wave stiffness, while the behavior of the $D0_3$ phase is qualitatively similar but quantitatively different. This difference is also clearly visible in the site-resolved dependencies in Fig. 5. In general, it is expected that Fe sites with different atomic environment may have different contributions to the total spin-wave stiffness. For the A2 phase, the site-resolved stiffness for Fe varies little for the whole range of Si concentrations. In the case of the B2 phase, both Fe sites show similar behavior (except for the smallest Si content of 2 at.%, see the discussion below) for Si concentrations up to 15 at.%. At higher Si concentrations, the contribution at the Fe(I) site starts to decrease while that of the Fe(II) remains constant. For the $D0_3$ phase, the variations are much stronger and the contribution from the Fe(III) sites shows an opposite trend than those from the Fe(I) and Fe(II) sites. While the Fe(III) contribution sharply increases for Si concentrations above 10 at.%, both the Fe(I) and Fe(II) contributions decrease.

In the following three subsections we analyze in more detail how the observed variations of the spin-wave stiffness relate to the changes of the lattice parameters, single-site magnetic moments, and the local electronic structure due to Si addition.

1. Volume interpretation

Figure 6 shows the variations of the spin-wave stiffness for the A2, B2, and $D0_3$ phases as functions of their equilibrium lattice parameters. While for the A2 phase the lattice parameter almost does not change with Si content, for both the B2 and $D0_3$ phases it decreases when the Si content exceeds 10 at.%. This result is consistent with previous KKR calculations of Khmelevska *et al.* [13]. According to experimental studies [30,31], the Si doping leads to approximately linear decrease of the equilibrium volume, which is more pronounced for the ordered $D0_3$ phases than for the A2 and B2 bcc phases. The

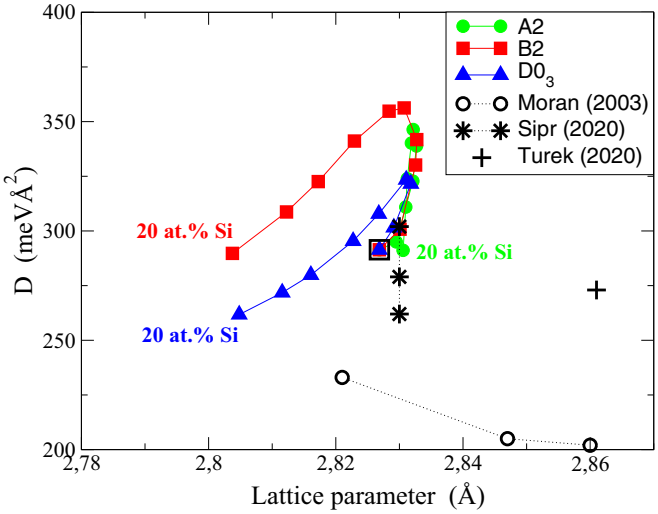

FIG. 6. Variations of the spin-wave stiffness for the A2, B2, and $D0_3$ phases with Si content from 0 to 20 at.% as a function of their equilibrium lattice parameters; the value corresponding to pure bcc Fe is marked by a black square. The graph also contains theoretical D values for bcc Fe from recent studies [18,19,32].

KKR calculations predict these trends qualitatively correctly, but only for Si concentrations exceeding 10 at.%.

Our value of D corresponding to pure bcc Fe (marked by an empty black square) is consistent with the recent detailed theoretical studies by Šipr *et al.* [18] and Turek *et al.* [19]. We also include theoretical results for bcc Fe obtained by Moran *et al.* [32] who observed a decreasing trend of D with increasing Fe lattice parameter. Our results for the B2 and $D0_3$ phases show an opposite trend, namely, a decrease of D with decreasing lattice parameter. However, as will be shown in the next two subsections, the volume effect is negligible compared to the changes induced by variations in the electronic structure.

2. Magnetic interpretation

To identify whether the trends in Fig. 5 are determined by the distribution of the single-site magnetic moments, we evaluated the $D_\alpha^{\mathrm{mag}}(x)$ contributions according to Eq. (9). The resulting dependencies are plotted for all nonequivalent Fe sites in all phases in Fig. 7. Contributions from the Si sites are smaller by one order of magnitude compared to those from the Fe sites and are therefore not considered.

The trends shown in Fig. 7 are consistent with those in Figs. 2 and 3 for all three phases. For the A2 phase, the increasing trend is due to the decreasing magnetic moment as a function of the Si concentration, as shown in Fig. 2. For the B2 phase, the magnetization at the Fe(I) site is roughly constant in the whole considered concentration range, while the Fe(II) site shows a strong decrease in the value of the magnetic moment (cf. Fig. 3). This is reflected in Fig. 7 where $D_\alpha^{\mathrm{mag}}(x)$ for Fe(I) changes only marginally while that for Fe(II) increases. Similar outcomes are obtained for the $D0_3$ phase, with Fe(I) and Fe(III) contributions remaining almost constant while that of Fe(II) increasing, again in accordance with the trends of Fig. 3. Hence, the increase in the value of $D_\alpha^{\mathrm{mag}}(x)$ upon Si

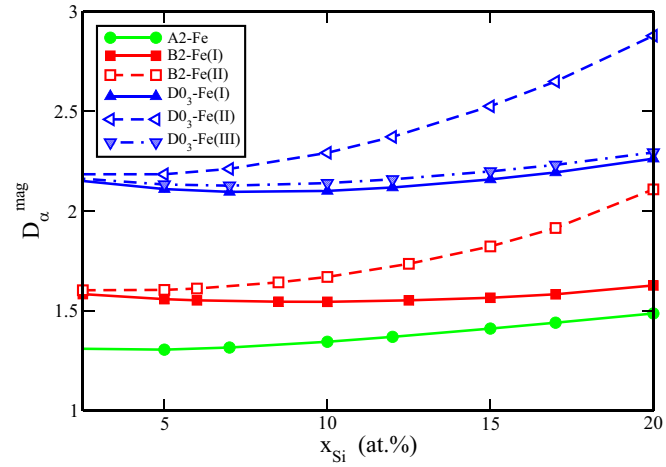

FIG. 7. Behavior of the function $D_\alpha^{\mathrm{mag}}(x)$ for Si concentration ranging from 2.5 to 20 at.% [it is singular at zero, see Eq. (9)].

doping for the Fe site in the A2 phase, and for the Fe(II) sites in both the B2 and $D0_3$ phases, is a direct consequence of the decreasing single-site magnetic moments on the corresponding sites. However, the $D_\alpha^{\mathrm{mag}}(x)$ dependencies do not show any correlation with the corresponding site-resolved contributions plotted in Fig. 5.

3. Electronic structure interpretation

In order to investigate the electronic structure effect on the exchange parameters and on the values of the spin-wave stiffness we plot the function $D_\alpha^{\mathrm{el}}(x)$ for all three phases in Fig. 8. The trends observed in Fig. 8 are clearly similar to those in Fig. 5. Hence, the spin-wave stiffness for the three Fe-Si phases is likely predominantly influenced by the changes of the electronic structure and hybridization mechanisms due to Si doping.

The analysis of the cumulative sum in Eq. (10) as a function of the distance from the origin can be used to understand the effect of Si on the decay of magnetic interactions,

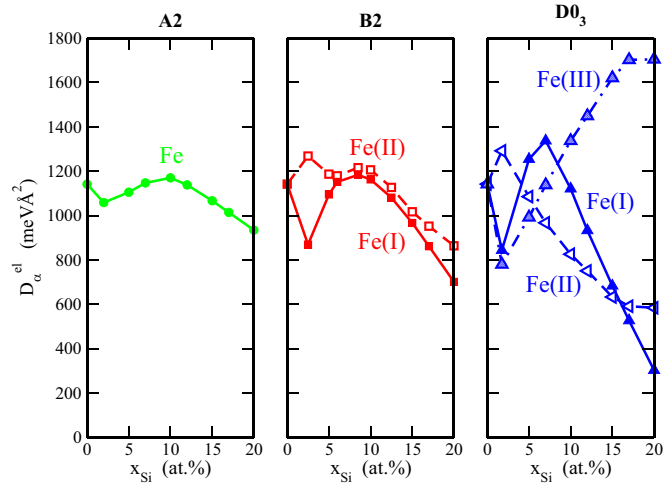

FIG. 8. Behavior of the function $D_\alpha^{\mathrm{el}}(x, \eta = 0.0)$ for the nonequivalent Fe sites of the A2, B2, and $D0_3$ phase.

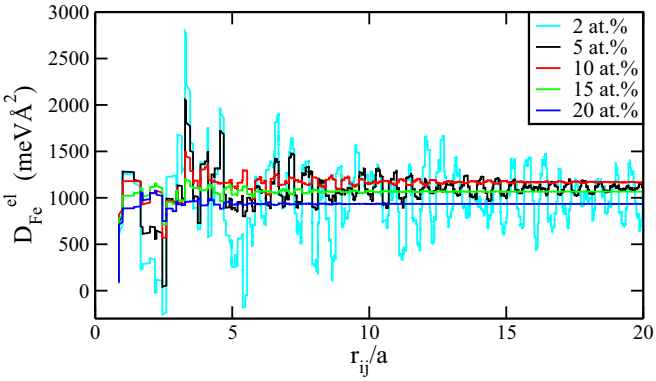

FIG. 9. Behavior of $D_\alpha^{\mathrm{el}}(x)$ for the A2 phase at different Si concentrations as a function of the distance r_{ij}/a from the central atom.

especially at large distances where in pure Fe the characteristic RKKY fluctuations are present. In addition, we can examine the changes of the exchange interactions at the Fe sites due to the hybridization with the orbitals of neighboring Si atoms. It has been shown [33,34] that the bonding states with the t_{2g} and e_g symmetries contribute in a different way to the total value of the exchange parameters in bcc Fe. The t_{2g} states, which are determined by the features of the Fermi surface, have a Heisenberg-like character and govern the RKKY oscillatory behavior. In contrast, the e_g states are short ranged, not Heisenberg-like, and determine the ferromagnetic behavior of the first coordination shell.

Figures 9, 10, and 11 display the cumulative sums from Eq. (10) as functions of the distance from the origin for the A2, B2, and $D0_3$ phases, respectively. For these plots we chose $\eta = 0.0$ (no damping) in order to discern clearly the changes

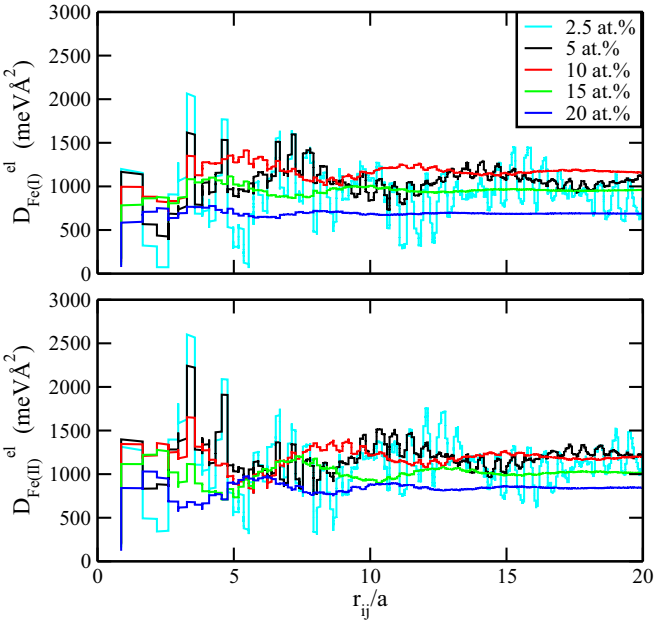

FIG. 10. Behavior of $D_\alpha^{\mathrm{el}}(x)$ for the Fe(I) and Fe(II) sites in the B2 phase at different Si concentrations as a function of the distance r_{ij}/a from the central atom.

in the fluctuations (the exponential damping smooths out the fluctuations, especially for larger values of η).

Figure 9 contains curves for Si concentrations from 2 to 20 at.%. At small concentrations (i.e., 2 and 5 at.%) one can see the typical RKKY fluctuating behavior that is damped only very slowly and does not decay even at the normalized distance of 20 lattice parameters. Hence, a large cutoff radius or the exponential damping is necessary to converge the sum, but the uncertainty in the spin-wave stiffness values for these small concentrations is still significant, approximately within ± 50 meV Å^2. For Si concentrations larger than 10 at.%, the RKKY oscillations are damped and the sums are well converged.

The results can be interpreted such that for small Si concentrations (i.e., $x < 10$ at.%) the RKKY oscillations are governing the value of the spin-wave stiffness, while for larger concentrations (i.e., $x > 10$ at.%) the value of D is mainly determined by the exchange interactions from the first few coordination shells and is not affected by more distant neighbors. In other words, the interactions between the t_{2g} Fe orbitals, which control the long-range behavior of J_{ij} [33,34], are effectively screened at larger Si concentrations.

The damping of long-range RKKY fluctuations upon Si doping makes the evaluation of the spin-wave stiffness easier and more reliable. For Si concentrations larger than 10 at.%, it is not necessary to avoid the ill-convergent summations by interpolations to zero damping. Converged results can therefore be obtained with a significantly shorter cutoff radius and less dense k mesh.

The results for the B2 and $D0_3$ phases are qualitatively similar to those of the A2 phase. The behavior of $c_{\mathrm{Fe(I)}}D_{\mathrm{Fe(I)}}$ and $c_{\mathrm{Fe(II)}}D_{\mathrm{Fe(II)}}$, shown in Fig. 5, is fully consistent with the trends of $D_\alpha^{\mathrm{el}}(x)$ plotted in Fig. 10 for different Si concentrations. Interestingly, for the B2 phase the RKKY fluctuations are damped less with increasing Si content than for the A2 phase, especially for the Fe(II) sites. Another notable point, most clearly visible for the black curves corresponding to 5 at.% of Si, is that the $D_\alpha^{\mathrm{el}}(x)$ fluctuations at the Fe(I) and Fe(II) sites have an opposite phase. This is likely related to the reciprocal arrangement of the coordination shells for the two sites.

The analysis of the cumulative sums for the $D0_3$ phase, shown in Fig. 11, is more complicated to perform, but it again offers a valuable tool to interpret the trends in Fig. 5. The overall behavior of $D_\alpha^{\mathrm{el}}(x)$ for the Fe(I) and Fe(II) sites is very similar to that found for the B2 phase. This is due to the fact that these two sites have similar local atomic environments in both phases, namely, the Fe(I) sites are partially occupied by Si while the Fe(II) sites have Si atoms in the first coordination shell. One can also notice that the dependencies for the Fe(II) and Fe(III) sites show an oscillatory behavior even at large Si concentrations. Hence, the long-range interactions are damped less effectively for these sites. The phase shift by a half period is again seen for the Fe(II) sites (as in the B2 phase) while the fluctuations at the Fe(I) and Fe(III) sites, which are located at the centers of the eight bcc cubes of the $D0_3$ phase, are in phase. The increasing value of $c_{\mathrm{Fe(III)}}D_{\mathrm{Fe(III)}}$ as a function of Si concentration (cf. Fig. 5) is consistent with the mean values of the $D_\alpha^{\mathrm{el}}(x)$ curves for the Fe(III) site in the bottom panel of Fig. 11.

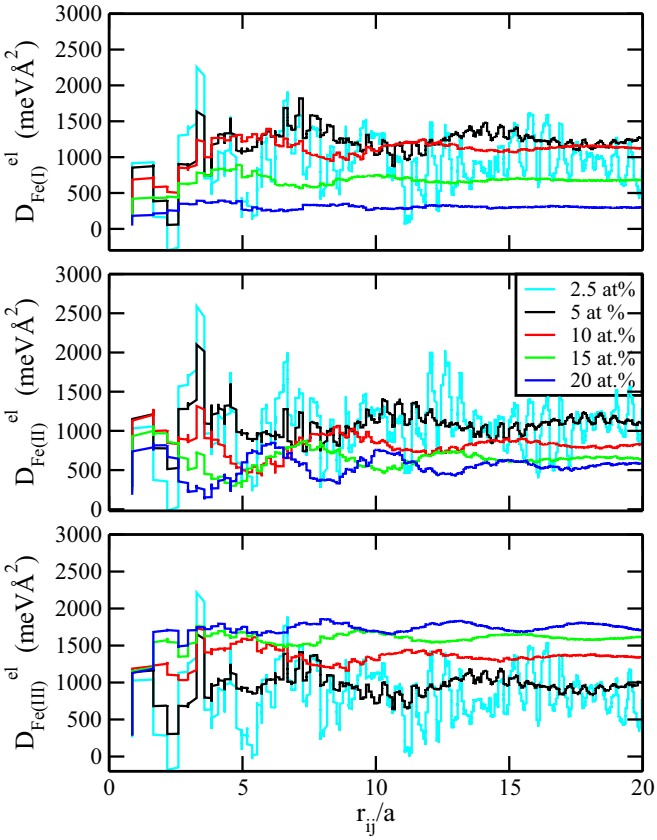

FIG. 11. Behavior of $D^{el}_{\alpha}(x)$ for the Fe(I), Fe(II), and Fe(III) sites in the $D0_3$ phase at different Si concentrations as a function of the distance r_{ij}/a from the central atom. The coloring of the lines is the same as in Fig. 10.

A complementary understanding of the changes in the electronic structure induced by the Si doping can be obtained from analysis of the electronic densities of states (DOS). The spin-wave stiffness is related to changes in the electronic structure associated with magnon excitations of small **q** vectors [35]. Therefore, perturbations in the DOS close to the Fermi level can be related to deviations in the value of D.

In Fig. 12 we plot integrated differences between DOS of the doped (with Si doping of 10 and 20 at.%) and undoped phases; B2 (left column) and $D0_3$ (right column). One can see that for the smaller doping of 10 at.% (dashed curves) the changes in the local occupations at all Fe sites are relatively small, especially at the Fermi level. This means that for this concentration there should be negligible changes in the site-resolved spin-wave stiffness, which is fully consistent with the results in Fig. 5. In contrast, for the doping of 20 at.% there is a strong decrease in the occupation on the Fe(I) sites, especially for the $D0_3$ phase. This is consistent with the large decrease of $c_{Fe(I)}D_{Fe(I)}$ in Fig. 5. However, a rather strong increase of $c_{Fe(III)}D_{Fe(III)}$ in the the $D0_3$ phase is not reflected by any significant changes in the DOS occupation in Fig. 12.

IV. DISCUSSIONS AND CONCLUSIONS

In this work we studied the behavior of the spin-wave stiffness upon Si doping in Fe-rich Fe-Si alloys. Three fundamental phases, namely disordered A2 and partially ordered B2 and $D0_3$, were investigated for Si concentrations ranging from 0 to 20 at.%. Our study employed electronic structure calculations based on the KKR-CPA framework that allowed us to examine different contributions to the total and site-resolved values of D. The obtained trends due to Si doping were analyzed in terms of volumetric effects, variations of local magnetic moments, and changes of the electronic structure.

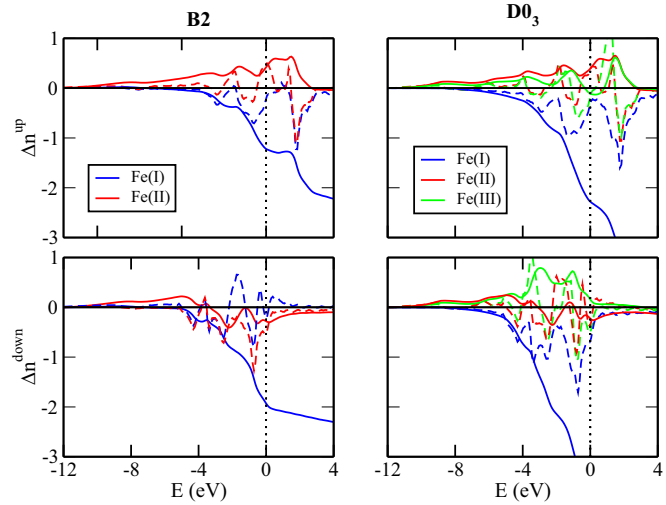

FIG. 12. Integrated differences of the spin-up and spin-down DOS between the doped and undoped B2 (left) and $D0_3$ (right) phases. The dashed and full curves correspond to Si doping of 10 and 20 at.%, respectively; the Fermi level corresponds to zero energy and is marked by the vertical dotted line.

The volumetric contribution, originating from the changes of the lattice parameter due to Si doping, was found not to correlate with the observed changes of the spin-wave stiffness. Similarly, the magnetic contribution, proportional to the inverse product of the single site magnetic moments, did not correspond with the trends of the total and site-resolved spin-wave stiffness. Hence, the primary cause of the variations was pinpointed to the changes of the electronic structure. Our analysis revealed that the site-resolved spin-wave stiffness is mostly controlled by the behavior of the exchange interactions. The exchange interactions between the t_{2g} Fe orbitals are strongly suppressed for Si concentrations larger than about 10 at.%. This efficient damping of the long-range RKKY fluctuations enables a more reliable determination of the spin-wave stiffness values, while for small Si concentrations an uncertainty of about 100 meV Å^2 remains, even for long cutoff values employed here. The observed trends in the local magnetic moments as well as the site-resolved spin-wave stiffness for the Fe(I) and Fe(II) sites are very similar in the B2 and $D0_3$ phases. This is related to their equivalent local atomic environments characterized by the number of Si neighbors. This similarity is also apparent in the changes of DOS for different Si doping levels.

Our theoretically predicted decrease in the total spin-wave stiffness for Si concentrations greater than about 8–10 at.%, as plotted in Fig. 4, is consistent with the available experimental data. However, there exist apparent quantitative discrepancies,

in particular for the A2 and B2 bcc phases. As mentioned above, the real space summation is difficult to converge for small Si concentrations due to the long-range RKKY oscillations and the uncertainty of the obtained values is rather large. The reported theoretical predictions for the spin-wave stiffness in pure bcc Fe range from 250 to 350 meV Å^2, and our value of 291 meV Å^2 agrees very well with values reported in the recent detailed comparative study by Šipr *et al.* [18]. Nevertheless, the initial increasing trend for Si concentrations up to 8–10 at.% obtained by our calculations may be an artifact caused by large uncertainties in the evaluations of the sum in Eq. (7). Moreover, as discussed recently by Turek *et al.* [19] for the Fe-Al system, a further improvement of the obtained trends can be achieved by including vertex corrections that may lower the value of the spin-wave stiffness, especially at high Si concentrations.

A proper comparison between theory and experiment also needs to take into account the changes in the local atomic ordering. Depending on the processing conditions, the Fe-Si alloys can undergo B2 and $D0_3$ type ordering for Si concentrations above 8–10 at.% and temperatures $T > T_c$ and $T < T_c$, respectively. It was reported already by one of the first experimental work by Antonini *et al.* [27] (gray circles in Fig. 4) that a large fraction of Fe_3Si ($D0_3$) ordering was present in their samples containing just 15 at.% of Si. The increase in the $D0_3$ short-range order for concentrations larger than 8 at.% was also confirmed by Gorbatov *et al.* [36] using Monte Carlo simulations performed at the ferromagnetic state. Such transformations are clearly relevant and could partly explain the quantitative discrepancies between the theoretical predictions and experimental data and the qualitative agreement of the experimental trends with that of the $D0_3$ phase.

ACKNOWLEDGMENTS

M.R. acknowledges support from the International Max Planck Research School for Interface Controlled Materials for Energy Conversion (IMPRS-SurMat) and from Robert Bosch GmbH, 71272 Renningen, Germany. The computations have been performed using the ZGH cluster at ICAMS and the Gamma and Triolith clusters, managed by the Swedish National Infrastructure for Computing (SNIC) at the National Supercomputer Centre (NSC) in Linköping.

APPENDIX A: DETERMINATION OF THE SPIN-WAVE STIFFNESS FOR THE ORDERED $D0_3$ PHASE FROM THE ADIABATIC MAGNON SPECTRUM

To prove the validity of our weighted averaging procedure [Eq. (8)] for structures with multiple sublattices, we computed the spin-wave stiffness for the ordered $D0_3$ phase directly from the curvature of the magnon spectrum.

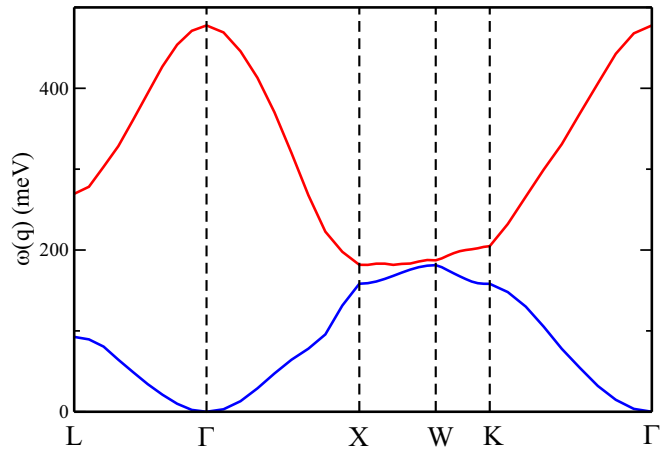

FIG. 13. Adiabatic magnon spectrum of the ordered $D0_3$ phase obtained by diagonalizing the 2×2 matrix in Eq. (A2) along the L-Γ-X-W-K-Γ path.

For structures with N nonequivalent sites, the magnon spectrum can be obtained by calculating the Fourier transforms of the exchange interactions between the atomic types μ and ν as [37]

$$J^{\mu\nu}(\mathbf{q}) = \sum_j J_{0j}^{\mu\nu} e^{i\mathbf{q}\cdot\mathbf{R}_{0j}}, \tag{A1}$$

where $J_{0j}^{\mu\nu}$ is the exchange interaction between the central atom 0 and its neighbor j. The dispersion relation $\omega(\mathbf{q})$ is then obtained by diagonalizing the following N × N matrix given in its block form as [37]

$$4\begin{pmatrix} \frac{1}{M_\mu}\sum_\alpha^N \left(J^{\mu\alpha}(\mathbf{0}) - J^{\mu\mu}(\mathbf{q})\right) & -\frac{J^{\mu\nu}(\mathbf{q})}{M_\mu} \\ -\frac{J^{\mu\nu}(\mathbf{q})^\star}{M_\nu} & \frac{1}{M_\nu}\sum_\alpha^N \left(J^{\alpha\nu}(\mathbf{0}) - J^{\nu\nu}(\mathbf{q})\right) \end{pmatrix}, \tag{A2}$$

where M_μ and M_ν are the magnetic moments of the atom types μ and ν.

In the case of the ordered $D0_3$ phase, the diagonalization of this matrix (Si contribution were neglected), gives the dispersion relation shown in Fig. 13 with one acoustic (blue) and one optical (red) branch. The obtained value of the spin-wave stiffness (corresponding to the curvature of the acoustic branch at the Γ point), equals to 183 meV Å^2, which is is consistent with the trend shown in Fig. 4.

[1] R. C. O'Handley, *Modern Magnetic Materials: Principles and Applications* (Wiley, New York, 2000).
[2] O. Kubaschewski, *Iron-Binary Phase Diagrams* (Springer Science & Business Media, New York, 2013).
[3] M. B. Stearns, Internal magnetic fields, isomer shifts, and relative abundances of the various Fe sites in FeSi alloys, Phys. Rev. **129**, 1136 (1963).
[4] M. B. Stearns, Measurement of conduction-electron spin-density oscillations in ordered FeSi alloys, Phys. Rev. B **4**, 4069 (1971).
[5] W. A. Hines, A. H. Menotti, J. I. Budnick, T. J. Burch, T. Litrenta, V. Niculescu, and K. Raj, Magnetization studies of binary and ternary alloys based on Fe_3 Si, Phys. Rev. B **13**, 4060 (1976).

[6] V. Niculescu, T. Burch, and J. Budnick, A local environment description of hyperfine fields and atomic moments in $Fe_{3-x}T_x$ Si alloys, J. Magn. Magn. Mater. **39**, 223 (1983).

[7] E. P. Elsukov, G. N. Konygin, V. A. Barinov, and E. V. Voronina, Local atomic environment parameters and magnetic properties of disordered crystalline and amorphous iron-silicon alloys, J. Phys.: Condens. Matter **4**, 7597 (1992).

[8] A. Williams, V. Moruzzi, C. Gelatt Jr, J. Kübler, and K. Schwarz, Aspects of transition-metal magnetism, J. Appl. Phys. **53**, 2019 (1982).

[9] J. Kudrnovský, N. E. Christensen, and O. K. Andersen, Electronic structures and magnetic moments of $Fe_{3+y}Si_{1-y}$ and $Fe_{3-x}V_xSi$ alloys with DO_3-derived structure, Phys. Rev. B **43**, 5924 (1991).

[10] E. G. Moroni, W. Wolf, J. Hafner, and R. Podloucky, Cohesive, structural, and electronic properties of Fe-Si compounds, Phys. Rev. B **59**, 12860 (1999).

[11] N. I. Kulikov, D. Fristot, J. Hugel, and A. V. Postnikov, Interrelation between structural ordering and magnetic properties in bcc Fe-Si alloys, Phys. Rev. B **66**, 014206 (2002).

[12] N. Ershov, Y. P. Chernenkov, V. Lukshina, V. Fedorov, and B. Sokolov, The structural origin of induced magnetic anisotropy in α-$Fe_{1-x}Si_x$ ($x = 0.05$–0.08) alloys, Phys. B: Condens. Matter **372**, 152 (2006).

[13] T. Khmelevska, S. Khmelevskyi, A. V. Ruban, and P. Mohn, Magnetism and origin of non-monotonous concentration dependence of the bulk modulus in Fe-rich alloys with Si, Ge and Sn: A first-principles study, J. Phys.: Condens. Matter **18**, 6677 (2006).

[14] N. Ershov, Y. Chernenkov, V. Lukshina, and V. Fedorov, Structure of α-FeSi alloys with 8 and 10 at.% silicon, Phys. Solid State **54**, 1935 (2012).

[15] A. Saengdeejing, Y. Chen, K. Suzuki, H. Miura, and T. Mohri, First-principles study on the dilute Si in bcc Fe: Electronic and elastic properties up to 12.5 at.% Si, Comput. Mater. Sci. **70**, 100 (2013).

[16] S. K. Bhattacharya, M. Kohyama, S. Tanaka, Y. Shiihara, A. Saengdeejing, Y. Chen, and T. Mohri, Mechanical properties of Fe rich Fe-Si alloys: *Ab initio* local bulk-modulus viewpoint, Mater. Res. Express **4**, 116518 (2017).

[17] Y. Choi, Y. Koo, S. Kwon, and L. Vitos, Ordered phases in Fe-Si alloys: A first-principles study, J. Korean Phys. Soc **72**, 737 (2018).

[18] O. Šipr, S. Mankovsky, and H. Ebert, Assessing different approaches to *ab initio* calculations of spin wave stiffness, Phys. Rev. B **101**, 134409 (2020).

[19] I. Turek, J. Kudrnovský, and V. Drchal, Methods of electron transport in *ab initio* theory of spin stiffness, Phys. Rev. B **101**, 134410 (2020).

[20] A. I. Liechtenstein, M. Katsnelson, V. Antropov, and V. Gubanov, Local spin density functional approach to the theory of exchange interactions in ferromagnetic metals and alloys, J. Magn. Magn. Mater. **67**, 65 (1987).

[21] A. I. Liechtenstein, M. Katsnelson, and V. Gubanov, Exchange interactions and spin-wave stiffness in ferromagnetic metals, J. Phys. F: Met. Phys. **14**, L125 (1984).

[22] A. I. Liechtenstein, M. Katsnelson, V. Antropov, and V. Gubanov, LSDF-approach to the theory of exchange interactions in magnetic metals, J. Magn. Magn. Mater. **54-57**, 965 (1986).

[23] H. Ebert, The SPRKKR package, version 7, https://www.ebert.cup.uni-muenchen.de/index.php/en/software-en/13-sprkkr (2014).

[24] M. Pajda, J. Kudrnovský, I. Turek, V. Drchal, and P. Bruno, *Ab initio* calculations of exchange interactions, spin-wave stiffness constants, and Curie temperatures of Fe, Co, and Ni, Phys. Rev. B **64**, 174402 (2001).

[25] J. Thoene, S. Chadov, G. Fecher, C. Felser, and J. Kübler, Exchange energies, Curie temperatures and magnons in Heusler compounds, J. Phys. D: Appl. Phys **42**, 084013 (2009).

[26] P. Dürrenfeld, F. Gerhard, J. Chico, R. K. Dumas, M. Ranjbar, A. Bergman, L. Bergqvist, A. Delin, C. Gould, L. W. Molenkamp, and J. Åkerman, Tunable damping, saturation magnetization, and exchange stiffness of half-Heusler NiMnSb thin films, Phys. Rev. B **92**, 214424 (2015).

[27] B. Antonini, F. Menzinger, A. Paoletti, and A. Tucciarone, Spin-wave dispersion relations in ferromagnetic Fe-Si Alloys, Phys. Rev. **178**, 833 (1969).

[28] H. A. Mook and R. M. Nicklow, Neutron scattering investigation of the magnetic excitations in iron, Phys. Rev. B **7**, 336 (1973).

[29] J. W. Lynn, Temperature dependence of the magnetic excitations in iron, Phys. Rev. B **11**, 2624 (1975).

[30] M. Polcarová, S. Kadečková, J. Bradler, K. Godwod, and J. Bak-Misiuk, Lattice parameters of FeSi alloy single crystals, Phys. Status Solidi A **106**, 17 (1988).

[31] E. Edmund, D. Antonangeli, F. Decremps, G. Morard, S. Ayrinhac, M. Gauthier, E. Boulard, M. Mezouar, M. Hanfland, and N. Guignot, Structure and elasticity of cubic Fe-Si alloys at high pressures, Phys. Rev. B **100**, 134105 (2019).

[32] S. Morán, C. Ederer, and M. Fähnle, *Ab initio* electron theory for magnetism in Fe: Pressure dependence of spin-wave energies, exchange parameters, and Curie temperature, Phys. Rev. B **67**, 012407 (2003).

[33] Y. O. Kvashnin, R. Cardias, A. Szilva, I. Di Marco, M. I. Katsnelson, A. I. Lichtenstein, L. Nordström, A. B. Klautau, and O. Eriksson, Microscopic Origin of Heisenberg and Non-Heisenberg Exchange Interactions in Ferromagnetic bcc Fe, Phys. Rev. Lett. **116**, 217202 (2016).

[34] R. Cardias, A. Szilva, A. Bergman, I. Di Marco, M. Katsnelson, A. Lichtenstein, L. Nordström, A. Klautau, O. Eriksson, and Y. O. Kvashnin, The Bethe-Slater curve revisited; new insights from electronic structure theory, Sci. Rep. **7**, 4058 (2017).

[35] O. Šipr, S. Mankovsky, and H. Ebert, Spin wave stiffness and exchange stiffness of doped permalloy via *ab initio* calculations, Phys. Rev. B **100**, 024435 (2019).

[36] O. Gorbatov, A. Kuznetsov, Y. Gornostyrev, A. Ruban, N. Ershov, V. Lukshina, Y. Chernenkov, and V. Fedorov, Role of magnetism in the formation of a short-range order in iron-silicon alloys, J. Exp. Theor. Phys. **112**, 848 (2011).

[37] O. Eriksson, A. Bergman, L. Bergqvist, and J. Hellsvik, *Atomistic Spin Dynamics: Foundations and Applications* (Oxford University Press, Oxford, 2017).